CRYSTAL GROWTH & DESIGN

Article

Cite This: Cryst. Growth Des. XXXX, XXX, XXX−XXX

pubs.acs.org/crystal

Pressure-Induced Structural Transition to the Polar Phase in $GdFe_3(BO_3)_4$

Igor S. Lyubutin,[†] Alexander G. Gavriliuk,[*,†,‡,⊥] Nikita D. Andryushin,[§,∥] Maksim S. Pavlovskiy,[§] Viktor I. Zinenko,[§] Marianna V. Lyubutina,[†] Ivan A. Troyan,[†] and Ekaterina S. Smirnova[†]

[†]Shubnikov Institute of Crystallography of FSRC "Crystallography and Photonics" RAS, 119333 Moscow, Russia

[‡]Institute for Nuclear Research, Russian Academy of Sciences, Troitsk, 108840 Moscow, Russia

[§]Kirensky Institute of Physics, Federal Research Center KSC SB RAS, 660036 Krasnoyarsk, Russia

[∥]Siberian Federal University, 660041 Krasnoyarsk, Russia

[⊥]REC Functional Nanomaterials, Immanuel Kant Baltic Federal University, 236041 Kaliningrad, Russia

ABSTRACT: The $GdFe_3(BO_3)_4$ crystal has attracted great interest as a magnetic-field-induced multiferroic. In this paper, we show that the multiferroic properties in this crystal can be induced by high pressure. At high pressures up to 50 GPa, created in diamond anvil cells, the structural and vibrational (phonon) properties of the $GdFe_3(BO_3)_4$ crystal were studied. The structural phase transition was detected at about 23−25 GPa by Raman and synchrotron Mössbauer (NFS) spectroscopy. First-principle calculations of the crystal lattice dynamics at pressures below and above the structural transition were carried out. It was established that at pressures above the structural transition, the space group *R*32 of $GdFe_3(BO_3)_4$ is changed to the polar space group *R*3, and the crystal becomes a ferroelectric. At the *R*32 → *R*3 transition, the displacement of the boron ion B(2) and oxygen O results in the formation of boron−oxygen $B(2)O_4$ tetrahedrons instead of the plane BO_3 triangles. Meanwhile, the triangle oxygen environment of boron in the site B(1) remains unchanged. The nearest environment of the gadolinium ion also changes significantly. Instead of six oxygen ions in the *R*32 phase, the nearest surroundings of Gd in the *R*3 phase consist of nine oxygen ions forming a complex polyhedron. A large hysteresis of the transition indicates that this crystal remains a ferroelectric with a decrease in pressure to about ambient pressure.

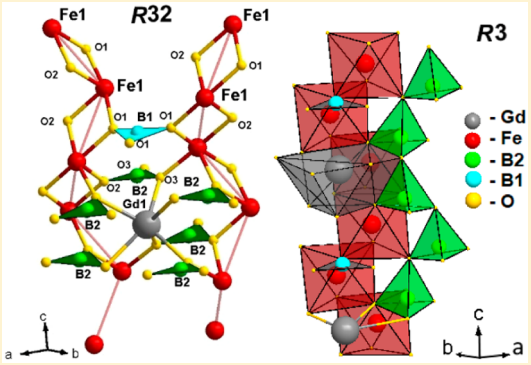

1. INTRODUCTION

The rare earth ferroborate $GdFe_3(BO_3)_4$, which has both 3d- and 4f-transition elements, is a rare magnetic material that is transparent in the visible range. Under ambient conditions, $GdFe_3(BO_3)_4$ is isostructural to the mineral huntite $CaMg_3(CO_3)_4$[1] and has trigonal symmetry with the space group *R*32.[2,3] The crystal structure of $GdFe_3(BO_3)_4$ can be represented by layers perpendicular to the *c*-axis (*C*3) and consisting of trigonal GdO_6 prisms and smaller FeO_6 octahedra.[2,3] The FeO_6 octahedra are connected by their edges and form helical one-dimensional weakly coupled chains extended along the *c*-axis.[3,4] The intrachain interactions between the Fe atoms are carried out via the Fe−O−Fe superexchange bonds. The magnetic interaction between the iron chains occurs through two oxygen atoms Fe−O−O−Fe, and a superexchange interaction along the Fe−O−Gd−O−Fe chain is also possible. It is clear that the main superexchange way of interaction between different iron chains is the path Fe−O−O−Fe, and that a slight distortion of this way can significantly change the magnetic properties of the system.

Boron atoms form isolated triangles with oxygen atoms, producing groups of two types. Triangles of type $B(1)O_3$ are connected by their vertices only to FeO_6 octahedra, while in a triangle of type B(2)O3, each of its two vertices is connected with a prism GdO6 and an FeO6 octahedron, and the third with two FeO6 octahedra.[4]

As a result of X-ray diffraction studies of a $GdFe_3(BO_3)_4$ single crystal at various temperatures, Klimin et al.[5] were the first who revealed a structural transition at about 90 K with lowering crystal symmetry from sp. gr. *R*32 (at 293 K) to $P3_121$ (below 90 K). This leads to the creation of two different helicoidal iron chains below 90 K. The appearance of two types of iron chains with different geometry at 90 K leads to a change in the magnetic properties of these crystals with a decrease in temperature.

Two low-temperature magnetic transitions: spin reorientation (spin flop) at T_{SR} = 9 K and antiferromagnetic-to-paramagnetic transition at the Neel temperature T_N = 38 K were observed in $GdFe_3(BO_3)_4$ by different magnetic and resonance methods.[6−14] It is assumed that below T_N magnetic

Received: May 11, 2019
Revised: September 3, 2019
Published: November 1, 2019

Downloaded via Alexander Gavriliuk on November 14, 2019 at 10:16:09 (UTC).
See https://pubs.acs.org/sharingguidelines for options on how to legitimately share published articles.

© XXXX American Chemical Society

DOI: 10.1021/acs.cgd.9b00609
Cryst. Growth Des. XXXX, XXX, XXX−XXX

ordering mainly relates to iron ions, whereas the Gd^{3+} ions are magnetized by the iron sublattice and substantially affect the anisotropic properties of the crystal.[7]

Currently, there is great interest in multiferroic compounds and mechanisms of magnetic−ferroelectric coupling in view of promising technological applications of such materials.[15] The practical importance of multiferroics for magnetic recording and spintronic devices is well-known;[16,17] however, to date only a few multiferroic crystals have parameters appropriate for practical use. The bismuth-ferrite ($BiFeO_3$) and rare-earth manganites ($RMnO_3$) with the perovskite-type crystal structure are the most famous. High excitement was caused by the discovery of a novel class of multiferroics in which ferroelectricity exists only in a magnetically ordered state.[16−20] In particular, some of the rare-earth iron borates [$RFe_3(BO_3)_4$] belong to this type of compound.

Recent studies have shown that the rare earth ferroborates $RFe_3(BO_3)_4$ (with R = Gd, Nd) are magnetic-field-induced multiferroics.[10,21,22] Electric polarization and magnetostriction in $GdFe_3(BO_3)_4$ appear at low temperatures as a result of a change in magnetic symmetry in the process of spin reorientation induced by an applied magnetic field (field-induced polarization - FIP).

To create materials of practical importance, the increase in critical temperatures of magnetic and ferroelectric transitions (T_N and T_P) is the key problem. Modification of the crystal structure by chemical engineering or/and by external pressure is the most promising way.

Under the influence of high pressures, structural and electronic phase transitions were revealed in a $GdFe_3(BO_3)_4$ crystal at pressures of about 25 and 43 GPa with an abrupt decrease in the optical gap and an insulator−semiconductor transition.[9] Thus, external actions lead to new effects and strongly influence the properties of the multiferroic $GdFe_3(BO_3)_4$.

The behavior of material at extreme conditions and the structural transformations play a key role in understanding its physical properties and designing new functions.

In this paper, the structural and vibration (phonon) properties of a $GdFe_3(BO_3)_4$ crystal subjected to high pressures were studied in diamond anvil cells. The structural phase transition in the pressure range of 23 GPa was studied by synchrotron Mössbauer spectroscopy at Fe-57 nuclei (nuclear forward resonance scattering - NFS) and Raman spectroscopy. The changes in the phonon spectra of a crystal during the structural transition was also investigated. An ab initio lattice dynamic calculation was carried out, and it was shown that at pressures above the structural transition, the crystal structure transforms into the polar phase and may have ferroelectric properties (electrical polarization).

2. EXPERIMENTAL AND CALCULATION METHODS

High-quality transparent, dark green single crystals of $GdFe_3(BO_3)_4$ were grown from solution in a melt.[23] Several typical crystals are shown in Figure 1. The crystal lattice parameters at ambient pressure are a = 9.5491(6) and c = 7.5741(5) Å.

For the Mössbauer spectroscopy studies, crystals with the Fe-57 isotope (enriched to 96%) were grown by the same technique.

In addition to X-ray diffraction, two experimental techniques, Raman spectroscopy and synchrotron Mössbauer spectroscopy (the nuclear forward scattering technique - NFS), were used to study structural transformations in $GdFe_3(BO_3)_4$ at high pressures.

Measurements at high pressures were performed in diamond anvil cells (DAC). The diameter of the diamond working area (cullet) was about 300 μm. The diameter of the hole in the gasket (rhenium foil), where the sample was placed, was about 100 μm. In the X-ray measurements, anvil supports were used with an output angle of 2θ of about 24.5 deg. The sample was made from powdered crystals by compacting the powder to a plate between the diamond anvils. Helium was used as the most hydrostatic pressure transmitting medium. Pressure calibration was performed by the ruby luminescence technique.

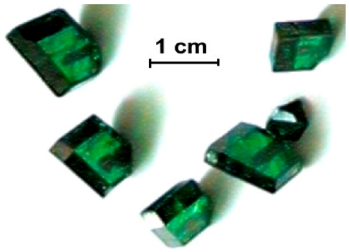

Figure 1. Several examples of the single crystals $GdFe_3(BO_3)_4$.

To obtain a thin sample for the NFS experiment, the single crystal was ground to powder, and a plate about 3.8 μm thick was prepared by prepressing the powder between the diamond anvils.

The plate of about 80 μm in diameter was placed in the working volume of the DAC, which was filled with argon (pressure transmitting medium). Pressure was measured by a standard ruby fluorescence technique. To control the pressure and its possible gradients across the diameter of the working volume in the DAC, several pieces of ruby about 1 μm in size were placed in the cell in addition to the sample.

NFS experiments were performed on the beamline 16-ID-D research synchrotron station in Argonne (APS, Argonne, United States). A 24-bunch operation mode was used in which pulses of the synchrotron beam were separated with a time interval of 154 ns. Resonant forward scattering spectra from ^{57}Fe nuclei (the time domain Mössbauer spectra[24]) were recorded at room temperature with increasing pressure up to P = 48 GPa.

For the Raman spectroscopy studies at high pressures, a $GdFe_3(BO_3)_4$ single crystal was used. The thickness of the crystal was about ∼10 μm. The sample with the lateral dimensions of about 80 × 40 μm^2 was placed into DAC with silicon oil (PES-5) as a pressure medium. In an optical microscope, the sample was transparent and almost colorless. Along with the sample, several ruby chips with dimensions of about 1 mm were placed in the cell at different distances from the sample center to evaluate the pressure gradient in the cell. The measurements were made at room temperature using the 488 nm and the 512 nm argon laser lines. The evolution of Raman spectra in $GdFe_3(BO_3)_4$ single crystal was measured at pressures up to 50 GPa in both compression and decompression regimes.

First principle calculations were carried out using the projector-augmented wave (PAW) method[20] within density functional theory (DFT), as implemented in the VASP code.[25−27]

We used the generalized gradient approximation (GGA) functional with Perdew−Burke−Ernzerhof (PBE) parametrization.[28] Electronic configurations were chosen as follows: Gd, $5p^6 5d^1 6s^2$; Fe, $3d^7 4s^1$; B, $2s^2 2p^1$; and O, $2s^2 2p^4$. 4f electrons of Gd were assumed as frozen in the core. The plane-wave cutoff was set at 600 eV. The size of the k-point mesh for the Brillouin zone, based on the Monkhorst−Pack scheme,[29] was 7 × 7 × 7. The GGA + U calculations, in the framework of the approach of Dudarev et al.,[30] were performed using the Hubbard potential for d states of Fe. Spin-polarized calculations were performed due to the presence of iron ions. The phonon spectra were calculated by constructing a supercell (2 × 2 × 2) and calculating the force constants using the small displacement method implemented in PHONOPY.[31]

DOI: 10.1021/acs.cgd.9b00609
Cryst. Growth Des. XXXX, XXX, XXX−XXX

3. RESULTS OF MEASUREMENTS AND PROCESSING

3.1. Mössbauer Spectroscopy Data. The evolution of the NFS spectra with increasing pressure is shown in Figure 2.

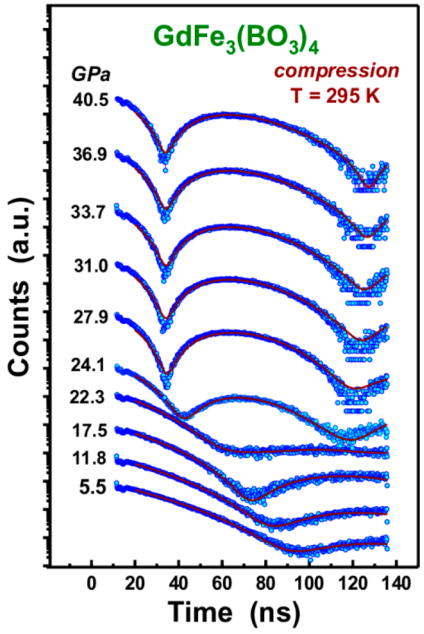

Figure 2. Evolution of the NFS spectra (dots) with increasing pressure at room temperature. The pressure transmitting medium in the DAC is argon. Solid lines are the calculated spectra with the approximation of the MOTIF program.

From the spectra, quantum beats are observed, which arise due to the modulation in time of the energy of scattered radiation during the decay of the excited state of the Fe-57 nuclei. This occurs when nuclear levels are split by hyperfine interaction into sublevels due to the interference between the scattered radiation components of different frequencies.[32]

At room temperature, the $GdFe_3(BO_3)_4$ crystal is in a paramagnetic state, and high-frequency quantum beats of a magnetic nature are not expected. The observed low-frequency beats are associated with electric quadrupole hyperfine splitting of the excited level of the ^{57}Fe nucleus (spin $I_{ex} = \pm 3/2$) into two sublevels. The period of quantum beats is inversely proportional to the magnitude of the hyperfine splitting.

The experimental NFS spectra were processed using the MOTIF program[33] (solid lines in Figure 2). The experiment clearly shows a change in the spectra at pressures of about 23 GPa, where the frequency of quantum beats sharply increases with increasing pressure, which indicates a phase transition. Figure 3 shows the dependence of the quadrupole splitting parameter (QS) on pressure, obtained from the NFS spectra. In the pressure range $0 < P < 20$ GPa, a slight increase in QS is observed, and then at $P = 23$ GPa, a sharp jump in QS occurs to a value of about 1.1 mm/s. Obviously, this is due to the structural phase transition, during which the collapse of the unit cell volume by 8% was detected.[34]

A significant increase in the QS parameter indicates a lowering in local symmetry in the environment of iron ions Fe^{3+} at this transition, and the appearance of strong distortions of the oxygen octahedra FeO_6. With a further increase in pressure up to 40 GPa, the value of QS does not change. We also measured several NFS spectra in the pressure reduction mode (see the dark triangles in Figure 3) and found that the

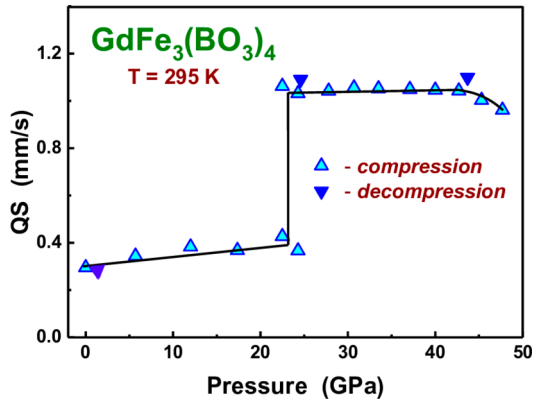

Figure 3. Dependence of the quadrupole splitting on the pressure, obtained from the NFS spectra, at room temperature. Solid lines are guides for the eye.

QS parameter values are restored to their original values at ambient pressure.

3.2. Raman Spectroscopy Data. The evolution of the Raman spectra during compression and decompression is shown in Figure 4a,b. In the compression regime, drastic

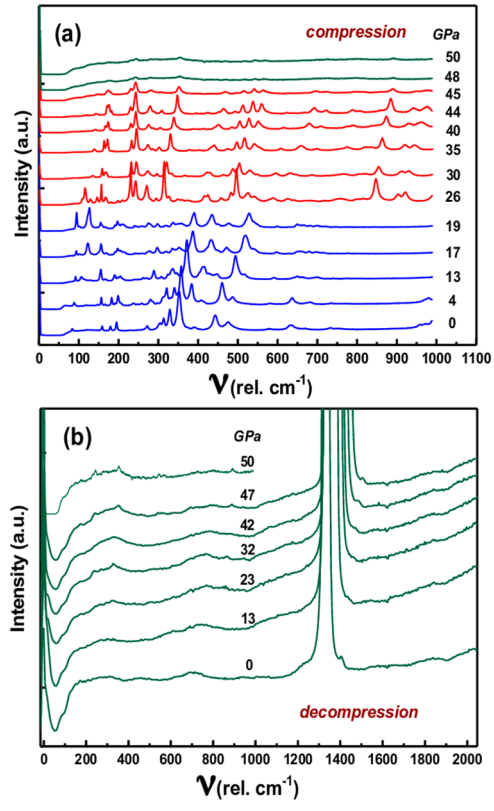

Figure 4. Evolution of Raman spectra in $GdFe_3(BO_3)_4$ at compression (a) and at decompression (b). Measurements were made at room temperature with the use of 488 and 512 nm lines of argon laser.

changes in the Raman patterns were revealed at pressures above 20 GPa and then at about 48 GPa (Figure 4a). The pressure dependence of the vibration frequencies in the $GdFe_3(BO_3)_4$ crystal under compression is shown in Figure 5.

The first anomaly at about 23 GPa correlates with the structural transition observed in our NFS experiments

DOI: 10.1021/acs.cgd.9b00609
Cryst. Growth Des. XXXX, XXX, XXX−XXX

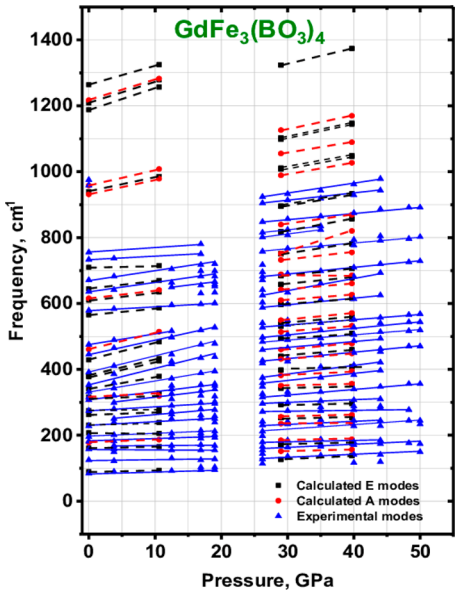

Figure 5. Dependence of the oscillation frequency of Raman-active modes on pressure. *A*-modes are red circles, *E*-modes are black squares, and experimental values are blue triangles. The experimental points are connected by solid lines, and calculated values are connected by dash lines.

presented above and with the XRD data previously obtained in ref 34. The second anomaly at about 48 GPa is accompanied by the disappearance of all Raman peaks, and patterns become amorphous-like. This anomaly correlates with the electronic transition observed previously in the optical absorption spectra of $GdFe_3(BO_3)_4$.[34]

As follows from the optical data, at this pressure, the energy of the optical gap decreases from 3.1 eV (at ambient pressure) to a value of ~0.7 eV, typical of semiconductors. Apparently, the disappearance of the Raman spectra above 48 GPa suggests the metallic character of the high-pressure structural phase of $GdFe_3(BO_3)_4$.

As seen in Figure 4b, Raman spectra are not restored under the decompression regime of measurements. A large hysteresis indicates that after the second transition, a new electronic state of the crystal remains metastable at ambient conditions.

3.3. Theoretical Analysis of the Raman Spectroscopy Data. The lattice dynamics was calculated using the computed lattice parameters and atomic coordinates corresponding to the minimum total energy. The lattice parameters and relative coordinates of the atoms, calculated in the present work and obtained experimentally in ref 4 for $GdFe_3(BO_3)_4$ in the *R*32 phase, are presented in Table 1. Good agreement between the calculated and experimental data is seen. Detailed results of the calculation of the lattice dynamics are presented in Table 2, as well as in Figure 5 and Figure 6.

The decomposition of an oscillatory presentation by irreducible representations in the center of the Brillouin zone has the form

$$\Gamma = 7A1 + 13A2 + 20E \quad (1)$$

Here, *A*1-type modes are the Raman-active modes, and *A*2 + *E* are the acoustic modes. The *A*2-type modes are the infrared IR-active modes and doubly degenerate *E*- type modes are active in both Raman and IR spectra.

Table 2 shows the calculated and experimental vibration frequencies for the center of the Brillouin zone, obtained in this work from the Raman spectra. In addition, the experimental values obtained from IR spectra in ref 35 are presented for comparison. As seen from Figure 5 and Table 2, the obtained values of the oscillation frequencies for the center of the Brillouin zone are in good agreement with the experimental data. An interesting feature of the calculated full phonon spectrum (Figure 6) is the absence of oscillation

Table 1. Relative Atomic Coordinates of Ions in a $GdFe_3(BO_3)_4$ Crystal (Space Group *R*32, Hexagonal Setting), Obtained by Calculation (at Ambient Pressure), and Experimental Data from Ref 4 Are Given for Comparison[a]

ion	Wyckoff position		*x/a*	*y/b*	*z/c*
Gd	3*a*	calc	0	0	0
		exp	0	0	0
Fe	9*d*	calc	0.2167	0.3333	0.3333
		exp	0.216576(9)	0.333333	0.333333
B1	3*b*	calc	0	0	0.5
		exp	0	0	0.5
B2	9*e*	calc	0.5523	0.5523	0.5
		exp	0.55248(7)	0.55248(7)	0.5
O1	9*e*	calc	0.1439	0.1439	0.5
		exp	0.14423(5)	0.14423(5)	0.5
O2	9*e*	calc	0.4085	0.4085	0.5
		exp	0.40883(6)	0.40883(6)	0.5
O3	18*f*	calc	0.0248	0.2115	0.1819
		exp	0.02540(4)	0.21261(5)	0.18268(5)

[a]The calculated unit cell parameters are a = 9.6251 Å and c = 7.6380 Å. The experimental unit cell parameters are a = 9.5554(1) Å and c = 7.5768(1) Å.[4].

Table 2. Vibration Frequencies for the Center of the Brillouin Zone (in cm^{-1}) of a $GdFe_3(BO_3)_4$ Crystal in the *R*32 Phase at Ambient Pressure[a]

E modes			A2 modes	
calc (this work)	Raman exp (this work)	IR TO [35]	calc (this work)	IR TO [35]
89	84.2	83.8	68	48.5
161	157.6	159.4	154	163.7
208	195.6	195.7	193	200.5
231	228.26	230.7	220	254.1
263		266.8	247	289.3
275	274.5	273.9	283	368.2
316	315.2	315.5	354	378.1
341	331.5	349.8	389	400
377	353.3	390.6	605	675.3
380	391.3	406.3	667	735.5
429	445.65	445	716	763.9
566	578.8	579.2	1242	1257.2
610	635.87	630.5	calc (this work)	Raman (this work)
644	671.2	669		
710	733.7	732.7	A1 modes	
940			178	182.1
	975.4	1202	309	307.1
1188		1223	461	475.5
1209		1287	616	
1264			931	
			958	959.0
			1217	

[a]TO is the transverse optical mode.

DOI: 10.1021/acs.cgd.9b00609
Cryst. Growth Des. XXXX, XXX, XXX−XXX

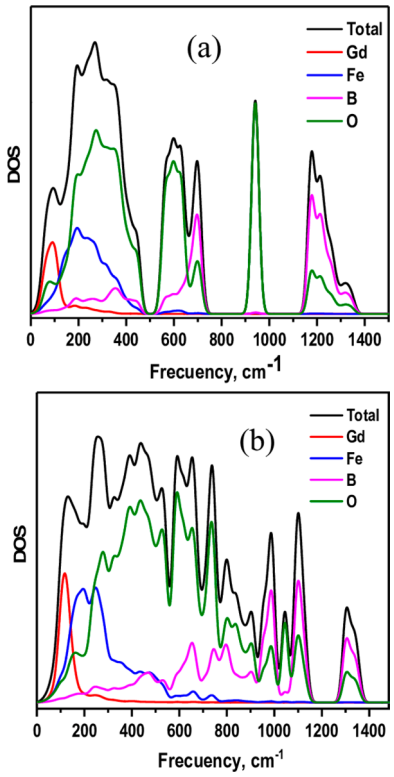

Figure 6. Density of phonon states of a $GdFe_3(BO_3)_4$ crystal in the *R*32 phase at ambient pressure (a) and in the *R*3 phase at a pressure of 30 GPa (b). The total density of states is the black line. The partial density of states is represented by lines: red for Gd ions, blue for Fe ions, pink for B ions, and green for O ions.

frequencies in a fairly wide range (750−950 cm^{-1}), which is also clearly seen in the experimental data of Figure 5. This feature is characteristic of compounds containing BO_3 triangles as structural elements, in the absence of BO_4 tetrahedra in the structure. In particular, this peculiarity is inherent in crystals with a huntite structure.

We measured using increasing pressure the Raman spectra only up to 1000 cm^{-1}. However, during the decompression regime, the spectra were measured to 2000 cm^{-1}. As seen in Figure 4b, in the region of 1200−1500 cm^{-1}, there is a very intense peak appearing from the diamond anvil. However, at full decompression, the additional weak peaks appear on the left and right shoulders of the center line, which can be associated with the calculated modes 1208, 1217, and 1263.9 cm^{-1}.

The low-frequency mode of type *A*2 in the $GdFe_3(BO_3)_4$ structure was observed in IR spectra;[35] however, it cannot be observed in the Raman spectra. According to our calculations, the polar mode of the *A*2 type is the lowest in the frequency spectrum at the center of the Brillouin zone.

To establish the effect of pressure on the phonon spectrum of $GdFe_3(BO_3)_4$ in the *R*32 phase, the lattice dynamics was calculated at applied pressures of 0−30 GPa. It was found that the frequency value of the low-frequency polar *A*2 mode (which is 68 cm^{-1} at ambient pressure, see Table 2) at the center of the Brillouin zone decreases (softened) when pressure is applied, and the frequency takes an imaginary value at pressures above 20 GPa. This indicates that the pressure-induced structural instability occurs in the *R*32 phase. Meanwhile, the applied pressure up to 20 GPa did not change qualitatively the calculated spectrum as a whole. The pressure dependence of the frequency of the polar mode is shown in Figure 7.

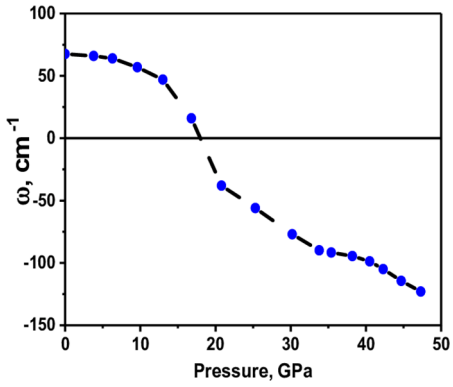

Figure 7. Pressure dependence of the frequency of the unstable polar mode. Imaginary frequencies are shown by negative values. Dashed line is a guide for the eye.

By displacing the ions in the cell in accordance with the eigenvector of the soft *A*2 mode, we calculated the change in the total energy of the $GdFe_3(BO_3)_4$ crystal. On the basis of the set of coordinates and lattice parameters of the distorted phase, the space group of this phase can be determined, for example, using the FINDSYM program.[36] Thus, we established that, at a pressure of 30 GPa, the distortion of the structure in the *R*32 phase by its eigenvector of the unstable polar mode is energetically favorable and leads to a structure with a space group of symmetry *R*3.

The change in the total crystal energy as a function of the amplitude of the ion displacement along the eigenvector of the soft mode is shown in Figure 8.

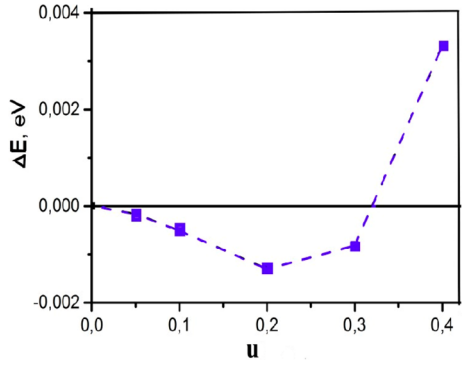

Figure 8. Dependence of the change in the total energy of a $GdFe_3(BO_3)_4$ crystal on the amplitude of ion displacements along the eigenvector of the soft mode. Dashed line is a guide for the eye.

The lattice dynamics calculation for $GdFe_3(BO_3)_4$ at pressure of 30 GPa was performed, and the full phonon spectrum for the *R*3 phase was constructed (Figure 9). The complete absence of unstable oscillation modes in the entire Brillouin zone can be seen in Figure 9, which indicates the stability of this structure.

The structure of the *R*3 phase, obtained by distorting the structure of the *R*32 phase along the eigenvector of the "soft" mode with u = 0.2 (see Figure 8), remains huntite-like. The ion displacements during the formation of the *R*3 phase

DOI: 10.1021/acs.cgd.9b00609
Cryst. Growth Des. XXXX, XXX, XXX−XXX

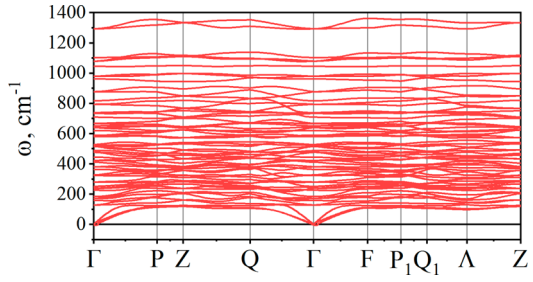

Figure 9. Full phonon spectrum of $GdFe_3(BO_3)_4$ in the *R*3 phase at a pressure of 30 GPa. *X*-axis: The standard designation of symmetric *k*-points of the first Brillouin zone for the rhombohedral lattice is used.

compared with the initial positions in the *R*32 phase do not exceed 0.04 Å. The subsequent relaxation of the structure of this *R*3 phase over the degrees of freedom of the ions at constant pressure leads to the formation of a new structure with the space group *R*3. Significant displacements of ions occur, leading to a change in the oxygen environment of boron and gadolinium ions (Figures 10, 11, 12, and 13). The lattice parameters and relative coordinates of the atoms in the new *R*3 phase at a pressure of 30 GPa are given in Table 3.

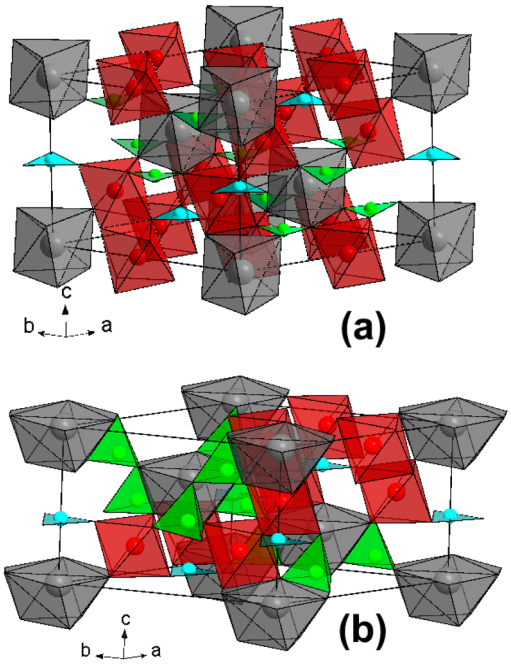

Figure 10. Crystal structure of $GdFe_3(BO_3)_4$. General view of the unit cell in the *R*32 (a) and *R*3 (b) phases.

The difference in energy (advantage) of the *R*3 phase, obtained by distorting the structure of the *R*32 phase along (over) the eigenvector of the "soft" mode with $u = 0.2$ (see Figure 8), with respect to the *R*32 phase energy is 0.0013 eV. Moreover, the difference in energy (advantage) of the *R*3 phase, obtained due to complete relaxation, from the energy of the *R*32 phase is 0.8 eV. Thus, the energy benefit (advantage) of the final *R*3 phase is 2 orders of magnitude greater than that for the *R*3 phase formed only by ferroelectric distortion.

General view of the unit cell of $GdFe_3(BO_3)_4$ in the *R*32 (a) and *R*3 (b) phases is shown in Figure 10. In the initial *R*32 structure, each boron ion in the sites B(1) (blue) and B(2) (green) is located in the center of a triangle formed by the

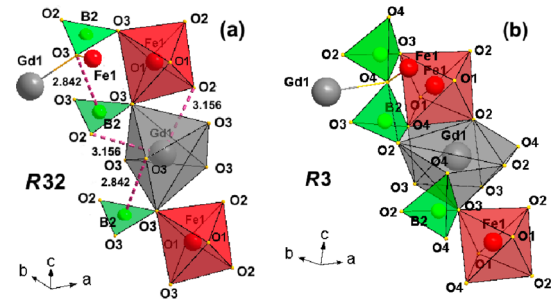

Figure 11. Changes in the geometry of the atomic structure in $GdFe_3(BO_3)_4$ during the transition from sp. gr. *R*32 (a) to sp. gr. *R*3 (b) at pressures above 25 GPa. The pink dashed lines in (a) show the distances between the atoms given in angstroms. The decrease in these distances with increasing pressure leads to the rebuilding of coordination polyhedra shown in (b).

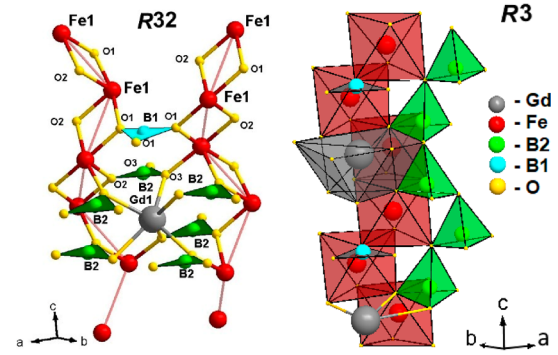

Figure 12. Comparative view of the $B(1)O_3$ and $B(2)O_3$ triangles in the *R*32 phase and $B(1)O_3$ triangle and $B(2)O_4$ tetrahedra in the *R*3 phase. In the sp. gr. *R*3, the $B(1)O_3$ triangles remain unchanged; the $B(2)O_4$ tetrahedra and FeO_6 octahedra create helicoidal chains. The GdO_9 polyhedron is also shown.

three nearest oxygen ions (Figure 10a). When the structure is rearranged to the *R*3 phase, the boron ion B(2) shifts along the *z* axis and moves out of the oxygen triangle plane. The displacement of oxygen ions during structural rearrangement leads to an increase in the number of nearby oxygen ions surrounding the boron ion in the position B(2) (Figures 10–13). In particular, the displacement of oxygen O(3) results in formation of the boron–oxygen tetrahedron $B(2)O_4$ with the boron ion in the center of the tetrahedron. Meanwhile, the nearest oxygen environment of the boron ion in the site B(1) does not change (Figure 12).

An initial triangle oxygen environment of B(2) in the *R*32 phase is shown in Figure 11a. In the *R*3 phase, boron $B(2)O_4$ tetrahedra are connected to each other by the O(4) vertex and form helicoidal chains along the *c* axes (Figures 12 and 13b). The pink dashed lines in Figure 11a show the distances between the atoms. The decrease in these distances with increasing pressure leads to the rebuilding of coordination polyhedra, and their new shapes are shown in Figures 11b, 12b, and 13. Each of the vertices of the $B(2)O_4$ tetrahedron is connected to the FeO_6 octahedron, and two edges are shared with different GdO_9 polyhedra. Meanwhile, the $B(1)O_3$ triangles remain isolated from the $B(2)O_4$ tetrahedra and share each vertex with two FeO_6 octahedra from the same chain (Figure 12).

The nearest environment of the gadolinium ion changes significantly (Figure 13c). Instead of six oxygen ions in the *R*32

DOI: 10.1021/acs.cgd.9b00609
Cryst. Growth Des. XXXX, XXX, XXX–XXX

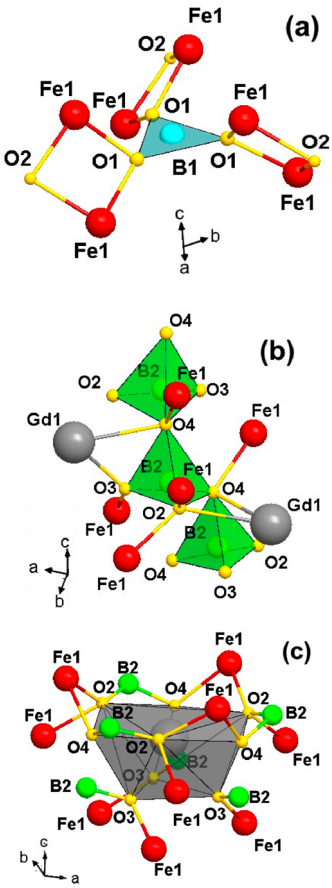

Figure 13. Local oxygen environment of the two types of boron ions B(1) (a) and B(2) (b) and gadolinium ions (c) in the crystal structure of $GdFe_3(BO_3)_4$ in the *R*3 phases.

Table 3. Calculated Relative Atomic Coordinates in $GdFe_3(BO_3)_4$ for the Space Group *R*3, Hexagonal Setting[a]

Ion	Wyckoff position	*x/a*	*y/b*	*z/c*
Gd	3*a*	0	0	0
Fe	9*b*	0.2484	0.3682	0.2462
B1	3*a*	0	0	0.4144
B2	9*b*	0.3568	0.1038	0.1393
O1	9*b*	0.1151	0.1630	0.3939
O2	9*b*	0.2991	0.2176	0.0807
O3	9*b*	0.5216	0.1599	0.0757
O4	9*b*	0.0602	0.2972	0.0444

[a]The obtained parameters of the unit cell are a = 9.2558 Å and c = 6.4696 Å.

phase, the nearest surroundings of Gd in the *R*3 phase consist of nine oxygen ions with the form of a complex polyhedron. The lower plane of coordination polyhedron is a triangle, and the upper plane is hexagon (Figure 13c). The Gd ion itself shifts along the z axis in the same direction as the boron ion.

Table 4 shows the calculated values of interatomic distances Fe−O and bond angles O−Fe−O for the $GdFe_3(BO_3)_4$ crystal in the *R*32 and *R*3 phases. These parameters are important for magnetic properties modified by high pressure. It is seen that the oxygen octahedron containing iron ions is essentially distorted in the *R*3 phase, which correlates with the experimental observation of a strong increase of the quadruple splitting parameter at the *R*32 → *R*3 transition shown in Figure 3. Meanwhile, the parameters of superexchange interactions Fe−O−Fe responsible for magnetic behavior are not improved, and an appreciable increase of the Neel temperature is not expected. In particular, the length of the Fe−O1 and Fe−O2 bonds, which provide superexchange between iron ions in chains along the c axis, increases in the *R*3 phase (see Table 4), while the bond angles Fe−O1−Fe and Fe−O2−Fe decrease from 103.5 to 96.3 and from 102.5 to 90.7 degrees during the transition of the *R*32 to *R*3 structure, respectively.

Table 4. Values of Interatomic Distances Fe−O and Bond Angles O−Fe−O in the $GdFe_3(BO_3)_4$ Crystal Calculated for the *R*32 and *R*3 Phases

*R*32	*d*, Å	*R*3	*d*, Å
Fe−O3	1.9894	Fe−O3	1.8447
Fe−O3	1.9894	Fe−O1	1.9234
Fe−O1	2.0393	Fe−O1	1.9359
Fe−O1	2.0393	Fe−O2	1.9909
Fe−O2	2.0536	Fe−O2	2.0033
Fe−O2	2.0536	Fe−O4	2.0065
*R*32	angle, deg	*R*3	angle, deg
O2−Fe−O3	86.6	O2−Fe−O3	83.7
O2−Fe−O2	87.4	O2−Fe−O2	85.7
O2−Fe−O3	86.6	O2−Fe−O4	95.4
O3−Fe−O3	101.4	O4−Fe−O3	95.3
O1−Fe−O2	76.9	O1−Fe−O2	90.7
O1−Fe−O2	94.3	O1−Fe−O2	91.9
O1−Fe−O3	95.6	O1−Fe−O4	87.2
O1−Fe−O3	91.9	O1−Fe−O4	93.6
O1−Fe−O3	95.6	O1−Fe−O3	95.2
O1−Fe−O3	91.9	O1−Fe−O3	88.6
O1−Fe−O2	76.9	O1−Fe−O2	90.7
O1−Fe−O2	94.3	O1−Fe−O2	80.5

To establish the value of pressure (P_{tr}) at which the structural phase transition occurs, the enthalpies of the *R*32 and *R*3 phases were calculated as a function of the applied hydrostatic pressure (Figure 14). The enthalpy was calculated using the formula for the thermodynamic potential $H = E_{tot} + PV$, where E_{tot} is the calculated total crystal energy, V is the cell volume, and P is the hydrostatic pressure. The transition pressure (P_{tr}) was determined by the intersection point of the enthalpy curves and amounted to 22 GPa (Figure 14). There is

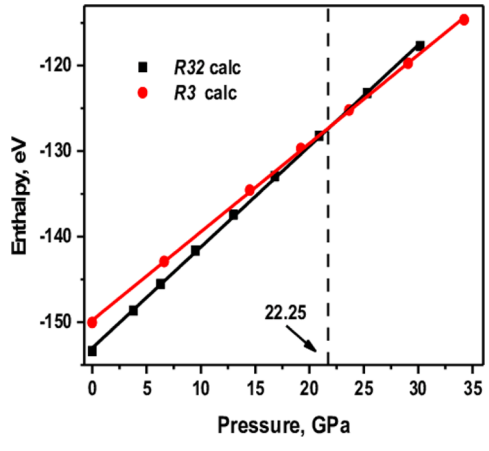

Figure 14. Pressure dependence of enthalpy of *R*32 phase (black curve) and *R*3 phase (red curve) in $GdFe_3(BO_3)_4$.

DOI: 10.1021/acs.cgd.9b00609
Cryst. Growth Des. XXXX, XXX, XXX−XXX

good agreement between this pressure value and the experimental transition pressure of about 25 GPa.[34]

4. DISCUSSION

The values of the Raman frequencies of $GdFe_3(BO_3)_4$ at different pressures, calculated for the center of the Brillouin zone, are shown in Figure 5 along with the experimental values. Obviously, there is good agreement between the calculated and experimental data at pressures both in the low pressure phase *R*32 and in the phase *R*3 at pressures above the structural transition.

Attention should be paid to filling the "gap" of frequencies (750−950 cm^{-1}) in the spectrum of the high-pressure phase, which was observed in the experiment. According to the calculated data, these frequencies correspond precisely to the vibrations of the boron−oxygen $B(2)O_4$ tetrahedra , which appear above the structural transition.

Here we note that, as it was indicated in book of Kazuo Nakamoto,[37] oscillation frequencies of the BO_3 and BO_4 molecules can be significantly different. In particular, for BO_3 they are 939, 740.5, 1330.0, 606.2 cm^{-1}, whereas for BO_4 they are 880, 372, 886, and 627 cm^{-1}.

The difference in the vibration properties of the $GdFe_3(BO_3)_4$ crystal in the *R*32 and *R*3 phases is more clearly represented in Figure 6, where the total and partial densities of phonon states are depicted for these phases. In the *R*3 phase, there are two peaks in the vicinity of the frequencies of 1050 and 1300 cm^{-1}, which persisted in the *R*32 phase in the vicinity of the frequencies of 950 and 1200 cm^{-1}. These peaks correspond to the oscillations of boron−oxygen triangles. In addition, two new peaks appear in the vicinity of the frequencies of 980 and 1100 cm^{-1}, related to vibrations of boron−oxygen $B(2)O_4$ tetrahedra (Figure 11b).

Crystal structures with both triangular and tetrahedral oxygen coordination of boron atoms are well-known, and, in particular, they can be found in $Li(BO_3)O_5$ and $K_2B_4O_7$. However, in borate crystals with a structure of type *R*3, which have stoichiometry BO_3, the simultaneous presence of triangles and tetrahedra was not known until now.

In general, the formation of structures with tetrahedra BO_4 is not unusual for boron-oxide crystals. In compounds with a chemical formula in which $(BO_3)_n$ can be singled out, as a rule, only BO_3 triangles are present in the structure (for example, $FeBO_3$, $Ca_3(BO_3)_2$). However, there are exceptions, for example, a YBO_3 crystal with only BO_4 tetrahedra in the structure.[38] Moreover, in the literature,[6] we found an example of $BaBi_2B_4O_{10}$ crystal, were BO_4 and BO_3 elements coexist. The structure of $BaBi_2B_4O_{10}$ is described in the monoclinic crystal system sp. gr. *P*21/*c*, and it is based on continuous boron−oxygen spirals twisted around the axis 21. In these spirals, the triborate groups of three tetrahedra $B(1)O_4$, $B(3)O_4$, and $B(4)O_4$ alternate with a $B(2)O_3$ triangle, which through vertex is connected to another triborate group. On the other hand, it should be indicated that investigations of such compounds under high pressure are very few. Thus, our discovery is a valuable contribution, opening the prospect of the formation of new structures under high pressure.

Figure 14 shows the pressure dependences of the unit cell volume of the crystal in the *R*32 and *R*3 phases, calculated in this work. At a calculated pressure equal to the transition pressure (22 GPa), the cell volume in the *R*3 phase is 10% less than the cell volume in the *R*32 phase. This is in good agreement well with the jump-like change in volume observed experimentally at the structural transition.[34]

Earlier, we studied the X-ray diffraction patterns of $GdFe_3(BO_3)_4$ under high hydrostatic pressures, and the structural phase transition was observed at about 25 GPa.[28] It was suggested that the crystal system does not change during this transition, whereas the unit cell volume changes abruptly by about 8%. However, it was impossible to determine the structure and space group.

Figure 15a,b shows the comparative behavior of the experimental and calculated curves of the unit cell volume

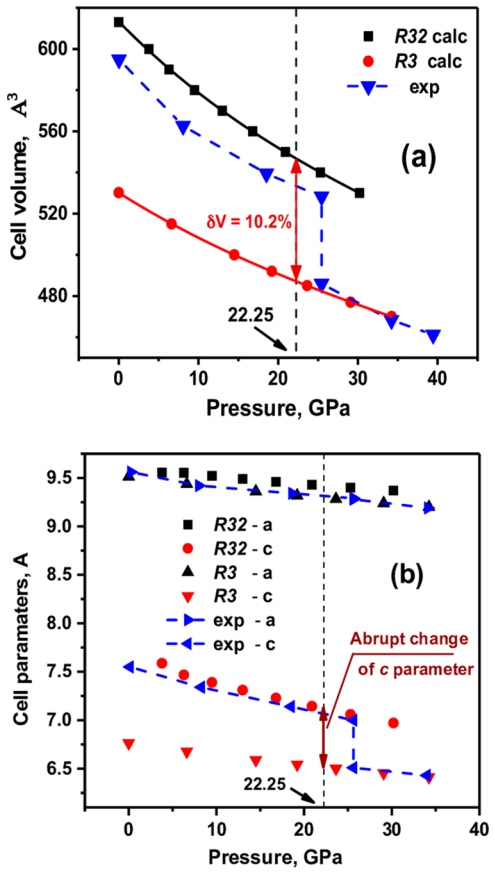

Figure 15. Pressure dependences of the unit cell volume (a) and the unit cell parameters (b) (represented in the hexagonal setting) of the $GdFe_3(BO_3)_4$ crystal. Black and red symbols and solid lines are the calculated data corresponding to the *R*32 and *R*3 phases, respectively. Blue symbols and dash lines are the experimental values.[34]

and parameters under the application of hydrostatic pressure, where the calculated curves are given for the crystal phases *R*32 and *R*3. As seen in Figure 15a, at a pressure equal to the calculated transition pressure (22 GPa), the cell volume in the *R*3 phase becomes 10% less than the cell volume in the *R*32 phase, which agrees well with the experiment.[34] The pressure behavior of the unit cell parameters (represented in the hexagonal setting in Figure 15b) in the phases *R*32 and *R*3 indicates that the lattice parameter *c* makes the largest contribution to the difference in cell volumes. The data obtained from the calculation, both qualitatively and quantitatively, are in good agreement with the experimental data.

DOI: 10.1021/acs.cgd.9b00609
Cryst. Growth Des. XXXX, XXX, XXX−XXX

5. CONCLUSION

The $GdFe_3(BO_3)_4$ crystal has attracted great interest as a magnetic-field-induced multiferroic.[10,21,22] Electric polarization and magnetostriction appear at low temperatures as a result of a change in magnetic symmetry during the spin reorientation induced by an applied magnetic field (field-induced polarization - FIP). In this paper, we have shown that multiferroic properties in such a crystal can be induced by high pressure.

Taking into account the results of calculations and, first of all, their good agreement with a wide range of experimental data, we can conclude that the structural phase transition occurring in $GdFe_3(BO_3)_4$ at high pressure is associated with lattice instability with respect to vibrations of the polar mode. Since the *R*3 phase is polar, it is possible to estimate the electric polarization in this phase, taking the *R*32 phase as the paraelectric phase. The obtained value, calculated from the displacements of ions and their charges, is 290 $\mu C/cm^2$.

At low temperatures, $GdFe_3(BO_3)_4$ is an antiferromagnet, and, obviously, at pressures of $P > 23$ GPa this crystal can be considered as a pressure-induced multiferroic (PIMF).

AUTHOR INFORMATION

Corresponding Author

*E-mail: gavriliuk@mail.ru.

ORCID

Alexander G. Gavriliuk: 0000-0003-0604-586X

Notes

The authors declare no competing financial interest.

ACKNOWLEDGMENTS

The authors express their deep gratitude to Prof. S. G. Ovchinnikov for initiating this work and fruitful discussions. These studies were performed with the support of the Ministry of Science and Higher Education within the State assignment FSRC ≪Crystallography and Photonics≫ RAS in part for the synchrotron Mössbauer measurements. Support from RFBR Grant No. 17-02-00766 in part for the Raman spectroscopy measurements and from No. 18-02-00696 in part for the theoretical calculations is also acknowledged. For preparation and tests of high-pressure cells,[39] the facilities of Center for Collective Use "Accelerator Center for Neutron Research of the Structure of Substance and Nuclear Medicine" of the INR RAS were used.

REFERENCES

(1) Campá, J. A.; Cascales, C.; Gutierrez-Puebla, E.; Monge, M. A.; Rasines, I.; Ruiz-Valero, C. Crystal structure, magnetic order, and vibrational behavior in iron rare-earth borates. *Chem. Mater.* **1997**, *9*, 237.

(2) Leonyuk, N. I.; Leonyuk, L. I. Growth and characterization of RM3(BO3)4 crystals. *Prog. Cryst. Growth Charact. Mater.* **1995**, *31*, 179.

(3) Leonyuk, N. I. Recent developments in the growth of RM3(BO3)4 crystals for science and modern applications. *Prog. Cryst. Growth Charact. Mater.* **1995**, *31*, 279.

(4) Smirnova, E. S.; Alekseeva, O. A.; Dudka, A. P.; Verin, I. A.; Artemov, V. V.; Bezmaternykh, L. N.; Gudim, I. A.; Frolov, K. V.; Lyubutin, I. S. Structure of Gd0.95Bi0.05Fe3(BO3)4 Single Crystals at 293 and 90 K. *Crystallogr. Rep.* **2016**, *61*, 558.

(5) Klimin, S. A.; Fausti, D.; Meetsma, A.; Bezmaternykh, L. N.; Van Loosdrecht, P. H. M.; Palstra, T. T. M. Evidence for differenciation in the iron-helicoidal chain in GdFe3(BO3)4. *Acta Crystallogr., Sect. B: Struct. Sci.* **2005**, *61*, 481−485.

(6) Balaev, A. D.; Bezmaternykh, L. N.; Gudim, I. A.; Temerov, V. L.; Ovchinnikov, S. G.; Kharlamova, S. A. Magnetic properties of trigonal GdFe3(BO3)4. *J. Magn. Magn. Mater.* **2003**, *258*, 532.

(7) Levitin, R. Z.; Popova, E. A.; Chtsherbov, R. M.; Vasiliev, A. N.; Popova, M. N.; Chukalina, E. P.; Klimin, S. A.; van Loosdrecht, P. H. M.; Fausti, D.; Bezmaternykh, L. N. Cascade of phase transitions in GdFe3(BO3)4. *JETP Lett.* **2004**, *79* (9), 423.

(8) Kharlamova, S. A.; Ovchinnikov, S. G.; Balaev, A. D.; Thomas, M. F.; Lyubutin, I. S.; Gavriliuk, A. G. Spin reorientation effects in GdFe3(BO3)4 induced by applied field and temperature. *J. Exp. Theor. Phys.* **2005**, *101*, 1098.

(9) Gavriliuk, A. G.; Lin, J.-F.; Lyubutin, I. S.; Struzhkin, V. V. Optimization of the conditions of synchrotron Mössbauer experiment for studying electronic transitions at high pressures by the example of (Mg, Fe)O magnesiowustite. *JETP Lett.* **2006**, *84* (3), 161.

(10) Yen, F.; Lorenz, B.; Sun, Y. Y.; Chu, C. W.; Bezmaternykh, L. N.; Vasiliev, A. N. Magnetic field effect and dielectric anomalies at the spin reorientation phase transition of GdFe3(BO3)4. *Phys. Rev. B: Condens. Matter Mater. Phys.* **2006**, *73*, No. 054435.

(11) Hinatsu, Y.; Doi, Y.; Ito, K.; Wakeshima, M.; Alemi, A. Magnetic and calorimetric studies on rare-earth iron borates LnFe3(BO3)4 (Ln = Y, La−Nd, Sm−Ho). *J. Solid State Chem.* **2003**, *172*, 438.

(12) Pankrats, A. I.; Petrakovskii, G. A.; Bezmaternykh, L. N.; Temerov, V. L. Antiferromagnetic resonance and magnetic anisotropy in single crystals of the YFe3(BO3)4-GdFe3(BO3)4 system. *Phys. Solid State* **2008**, *50*, 79.

(13) Mo, H.; Nelson, C. S.; Bezmaternykh, L. N.; Temerov, V. T. Magnetic structure of the field-induced multiferroic GdFe3(BO3)4. *Phys. Rev. B: Condens. Matter Mater. Phys.* **2008**, *78*, 214407.

(14) Frolov, K. V.; Lyubutin, I. S.; Smirnova, E. S.; Alekseeva, O. A.; Verin, I. A.; Artemov, V. V.; Kharlamova, S. A.; Bezmaternykh, L. N.; Gudim, I. A. Low-temperature structural and magnetic phase transitions in multiferroic GdFe3(BO3)4. *J. Alloys Compd.* **2016**, *671*, 545−551.

(15) Cheong, S.-W.; Mostovoy, M. Multiferroics: a magnetic twist for ferroelectricity. *Nat. Mater.* **2007**, *6*, 13.

(16) Kimura, T.; Goto, T.; Shintani, H.; Ishizaka, K.; Arima, T.; Tokura, Y. Magnetic control of ferroelectric polarization. *Nature* **2003**, *426*, 55−58.

(17) Hur, N.; Park, S.; Sharma, P. A.; Ahn, J. S.; Guha, S.; Cheong, S. W. Electric polarization reversal and memory in a multiferroic material induced by magnetic fields. *Nature* **2004**, *429*, 392−5.

(18) Pikin, S. A.; Lyubutin, I. S. Phenomenological model of multiferroic properties in langasite-type crystals with a triangular magnetic lattice. *Phys. Rev. B: Condens. Matter Mater. Phys.* **2012**, *86*, No. 064414.

(19) Lyubutin, I. S.; Pikin, S. A. Coexistence of spiral magnetic state and weak ferromagnetism in a multiferroic, cross-controlled by external magnetic and electric fields. *J. Phys.: Condens. Matter* **2013**, *25*, 236001.

(20) Khomskii, D. I. Classifying multiferroics: Mechanisms and effects. *Physics* **2009**, *2*, 20.

(21) Zvezdin, A. K.; Krotov, S. S.; Kadomtseva, A. M.; Vorob'ev, G. P.; Popov, Y. F.; Pyatakov, A. P.; Bezmaternykh, L. N.; Popova, E. A. Magnetoelectric effects in gadolinium iron borate GdFe3(BO3)4. *JETP Lett.* **2005**, *81*, 272.

(22) Zvezdin, A. K.; Vorob'ev, G. P.; Kadomtseva, A. M.; Popov, Y. F.; Pyatakov, A. P.; Bezmaternykh, L. N.; Kuvardin, A. V.; Popova, E. A. Magnetoelectric and magnetoelastic interactions in NdFe3(BO3)4 multiferroics. *JETP Lett.* **2006**, *83*, 509.

(23) Bezmaternykh, L. N.; Kharlamova, S. A.; Temerov, V. L. Flux crystallization of trigonal GdFe3(BO3)4 competing with the crystallization of α-Fe2O3. *Crystallogr. Rep.* **2004**, *49*, 855.

(24) Ruffer, R.; Chumakov, A. I. Nuclear resonance beamline at ESRF. *Hyperfine Interact.* **1996**, *97-98*, 589.

(25) Kresse, G.; Joubert, D. From ultrasoft pseudopotentials to the projector augmented-wave method. *Phys. Rev. B: Condens. Matter Mater. Phys.* **1999**, *59*, 1758.

DOI: 10.1021/acs.cgd.9b00609
Cryst. Growth Des. XXXX, XXX, XXX−XXX

(26) Kresse, G.; Furthmüller, J. Efficient iterative schemes for ab initio total-energy calculations using a plane-wave basis set. *Phys. Rev. B: Condens. Matter Mater. Phys.* **1996**, *54*, 11169.
(27) Kresse, G.; Furthmüller, J. Efficiency of ab-initio total energy calculations for metals and semiconductors using a plane-wave basis set. *Comput. Mater. Sci.* **1996**, *6*, 15.
(28) Perdew, J. P.; Burke, K.; Ernzerhof, M. Generalized Gradient Approximation Made Simple. *Phys. Rev. Lett.* **1996**, *77*, 3865.
(29) Monkhorst, H. J.; Pack, J. D. Special points for Brillouinzone integrations. *Phys. Rev. B* **1976**, *13*, 5188.
(30) Dudarev, S. L.; Botton, G. A.; Savrasov, S. Y.; Humphreys, C. J.; Sutton, A. P. Electron-energy-loss spectra and the structural stability of nickel oxide: An LSDA+U study. *Phys. Rev. B: Condens. Matter Mater. Phys.* **1998**, *57*, 1505.
(31) Togo, A.; Tanaka, T. First principles phonon calculations in materials science. *Scr. Mater.* **2015**, *108*, 1.
(32) Smirnov, G. V. *Hyperfine Interact.* **1999**, *123/124*, 31.
(33) Shvyd'ko, Y. V. MOTIF: Evaluation of time spectra for nuclear forward scattering. *Hyperfine Interact.* **2000**, *125*, 173.
(34) Gavriliuk, A. G.; Kharlamova, S. A.; Lyubutin, I. S.; Troyan, I. A.; Ovchinnikov, S. G.; Potseluiko, A. M.; Eremets, M. I.; Boehler, R. Structural and electronic transitions in gadolinium iron-borate GdFe3(BO3)4 at high pressures. *JETP Lett.* **2004**, *80* (6), 426−432.
(35) Klimin, S. A.; Kuzmenko, A. B.; Kashchenko, M. A.; Popova, M. N. Infrared study of lattice dynamics and spin-phonon and electron-phonon interactions in multiferroic TbFe3(BO3)4 and GdFe3(BO3)-4. *Phys. Rev. B: Condens. Matter Mater. Phys.* **2016**, *93*, No. 054304.
(36) Stokes, H. T.; Hatch, D. M. FINDSYM: Program for identifying the space group symmetry of a crystal. *J. Appl. Crystallogr.* **2005**, *38*, 237−238.
(37) Nakamoto, K. *Infrared and Raman Spectra of Inorganic and Coordination Compounds*; John Wiley & Sons, Inc., 2009.
(38) Lin, J.; Sheptyakov, D.; Wang, Y.; Allenspach, P. Structures and Phase Transition of Vaterite-Type Rare Earth Orthoborates: A Neutron Diffraction Study. *Chem. Mater.* **2004**, *16*, 2418.
(39) Gavriliuk, A. G.; Mironovich, A. A.; Struzhkin, V. V. Miniature diamond anvil cell for broad range of high pressure measurements. *Rev. Sci. Instrum.* **2009**, *80*, No. 043906.

DOI: 10.1021/acs.cgd.9b00609
Cryst. Growth Des. XXXX, XXX, XXX−XXX